Electronic Supplementary Information

A 9R-Like 2D Hybrid Metal Halide with Remarkably Low Melting Temperature

Wei Wang, Jing-Meng Zhang, Ming-Liang Jin, Chang-Qing Jing, Wen Zhang*

Jiangsu Key Laboratory for Science and Applications of Molecular Ferroelectrics and School of Chemistry and Chemical Engineering, Southeast University, Nanjing 211189, China.

Email: zhangwen@seu.edu.cn

Experimental section

Starting materials. 2-(methylamino)ethan-1-ol (98%), lead bromide ($PbBr_2$, 99.9%), and hydrobromic acid (HBr, 48 *wt*.% in H_2O) were commercially available and used as received without further purification.

Synthesis of $(MHEA)_4Pb_3Br_{10}$. $PbBr_2$ powder (9 mmol, 3.303 g) was dissolved in a solution comprising 4 mL of aqueous HBr. Following this, 2-(methylamino)ethan-1-ol (12 mmol, 0.901 g) was introduced into the solution. Subsequently, the clear solution was cooled and kept at 0 ℃ without any interference. During the process, colorless rod-like crystals began to precipitate at the bottom of the beaker. The solution was left for several days to facilitate further crystal growth. Afterward, the crystals were collected via suction filtration and dried in ambient air.

General Characterizations: PXRD patterns were obtained using a Rigaku SmartLab X-ray diffraction system. TGA was conducted with a NETZSCH TG209 F3 instrument at a heating rate of 10 °C min^{-1} in a nitrogen atmosphere. DSC measurements were performed using a NETZSCH DSC 214 Polyma instrument, also at a standard scan rate of 10 °C min^{-1}, unless noted otherwise. Ultraviolet-visible diffuse reflection spectra were recorded with a Shimadzu UV2600 spectrophotometer equipped with an ISR-2600Plus integrating sphere. Fourier-transform infrared spectra were collected using a Nicolet iS50 instrument through a transmission method. The viscosity was measured using a Thermo HAAKE MARS 60 with a 25 mm parallel plate, the cooling and shear rates are 10 K/min and 10 s^{-1}, respectively.

Single-Crystal X-ray Diffraction. Crystallographic data for the compound was gathered using a Rigaku Oxford Diffraction Supernova Dual Source, Cu at Zero, which is equipped with an AtlasS2 CCD and an XtaLAB Synergy R, DW system, HyPix diffractometer utilizing Mo Kα radiation. The data collection, cell refinement, and reduction were performed using the Rigaku CrysAlisPro software. Structure solution was achieved via direct methods using the SHELXL-2014 package, with all non-hydrogen atoms refined anisotropically. The crystallographic data can be found in the Cambridge Crystallographic Data Centre (CCDC number 2391828).

Theoretical calculations. Density Functional Theory (DFT) calculations were conducted using the

Vienna ab initio Simulation Package (VASP).[1] The input structures were derived from the crystallographic data and subsequently optimized with the cell fixed. Thresholds of convergence criteria are set as 10^{-7} eV and 0.02 eV/Å for energy differences during electronic steps and maximum forces in geometry optimization. The Perdew–Burke–Ernzerhof (PBE) functional, implemented within the generalized gradient approximation (GGA), was utilized to model the exchange-correlation interactions.[2,3] DFT-D3 method was used to evaluate the van der Waals interactions.[4] Ion-electron interactions were represented using projector augmented wave (PAW) potentials with an energy cutoff of 500 eV. Postprocessing analysis was performed using VASPKIT.[5]

References

(1) Kresse, G.; Furthmüller, J. Efficient Iterative Schemes for Ab Initio Total-Energy Calculations Using a Plane-Wave Basis Set. *Phys. Rev. B* **1996**, *54*, 11169-11186.

(2) Blöchl, P. E. Projector Augmented-Wave Method. *Phys. Rev. B* **1994**, *50*, 17953-17979.

(3) Perdew, J. P.; Burke, K.; Ernzerhof, M. Generalized Gradient Approximation Made Simple. *Phys. Rev. Lett.* **1996**, *77*, 3865-3868.

(4) Grimme, S.; Antony, J.; Ehrlich, S.; Krieg, H. A Consistent and Accurate Ab Initio Parametrization of Density Functional Dispersion Correction (DFT-D) for the 94 Elements H-Pu. *J. Chem. Phys.* **2010**, *132*, 154104.

(5) Wang, V.; Xu, N.; Liu, J.-C.; Tang, G.; Geng, W.-T. Vaspkit: A User-Friendly Interface Facilitating High-Throughput Computing and Analysis Using Vasp Code. *Comput. Phys. Commun.* **2021**, *267*, 108033.

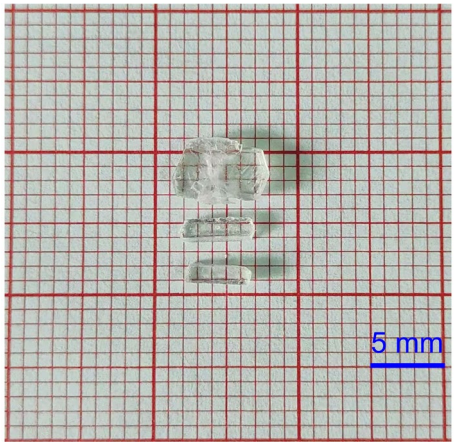

Fig. S1 Bulk single crystals of $(MHEA)_4Pb_3Br_{10}$

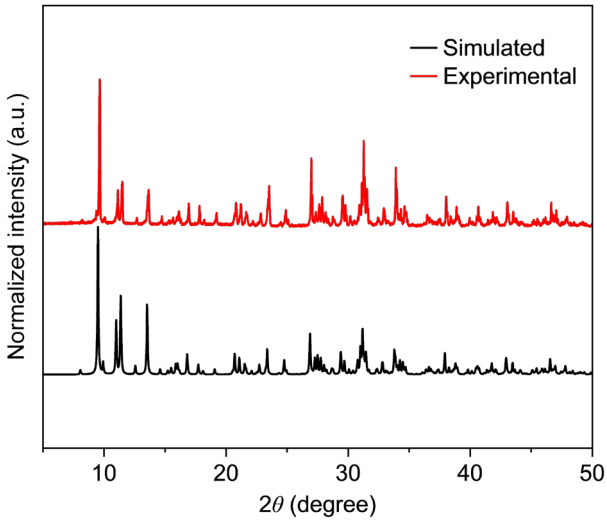

Fig. S2 PXRD pattern of $(MHEA)_4Pb_3Br_{10}$ powders.

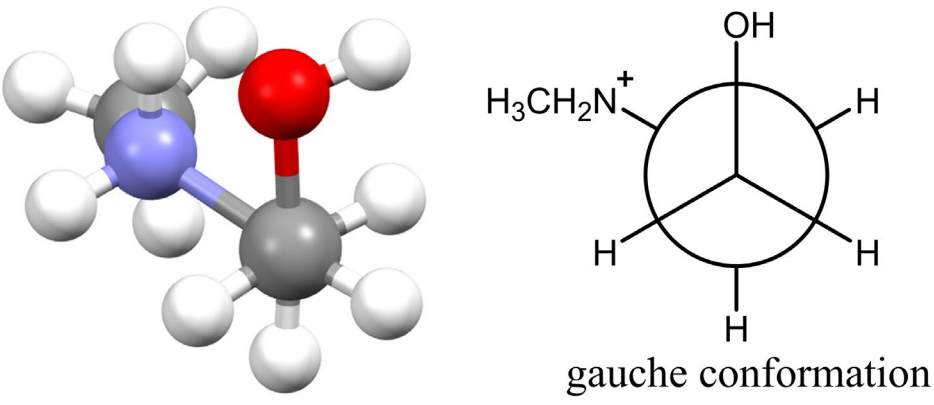

Fig. S3 Conformation analysis of MHEA cation.

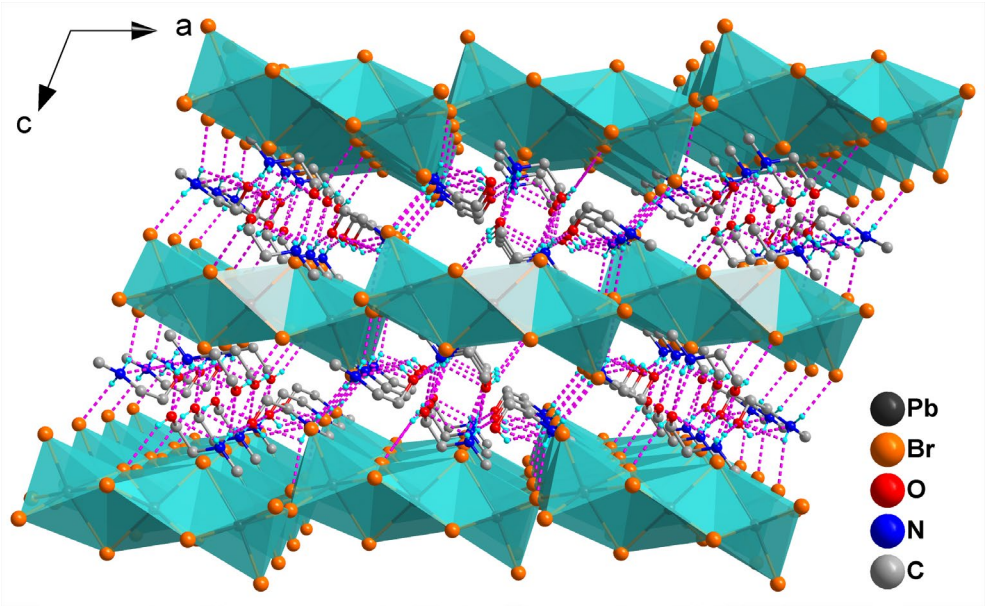

Fig. S4 Diagrams of supramolecular frameworks of crystal $(MHEA)_4Pb_3Br_{10}$ with hydrogen bonds.

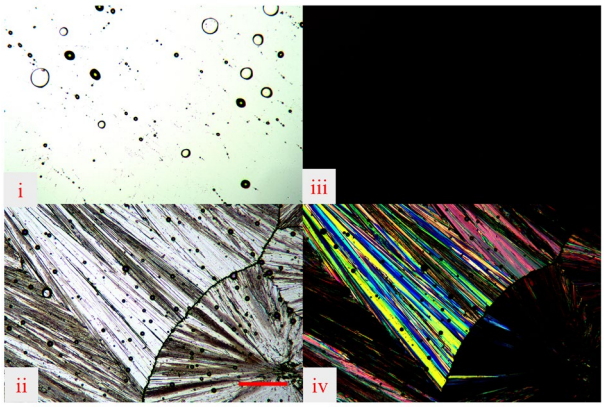

Fig. S5 Images of melts, and recrystallized crystals (from melts) under unpolarized light (i, ii) and cross-polarized light (iii, iv), respectively. Scale bar: 200 μm.

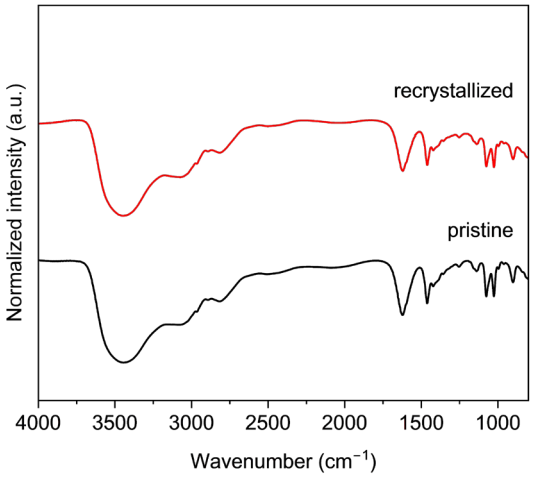

Fig. S6 IR spectra of fresh crystal and melt-processed powders.

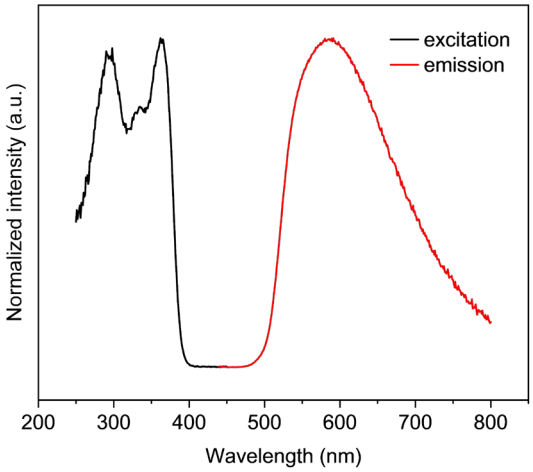

Fig. S7 Excitation and emission spectra of $(MHEA)_4Pb_3Br_{10}$.

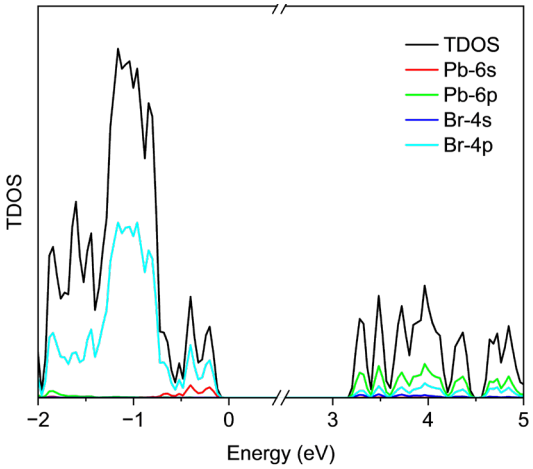

Fig. S8 Density of states of $(MHEA)_4Pb_3Br_{10}$.

Table S1 Crystallographic data and refinement parameters of $(MHEA)_4Pb_3Br_{10}$.

	$(MHEA)_4Pb_3Br_{10}$
***T* / K**	293(2)
Formula	$(C_3H_{10}NO)_4Pb_3Br_{10}$
Formula weight	1725.15
Crystal system	monoclinic
Space group	*C*2/*c*
***a* / Å**	23.6054(10)
***b* / Å**	8.6447(3)
***c* / Å**	20.0369(9)
***α* /°**	90
***β*/ °**	111.785(5)
***γ* /°**	90
Volume /Å^3	3796.8(3)
Z	4
D_{calc} /g·cm^{-3}	3.018
μ / mm^{-1}	23.817
***F*(000)**	3072.0
2θ range /°	4.378−49.994
Reflns collected	18759
Independent reflns (R_{int})	3338 (0.0814)
no. parameters	155
GOF	1.080
R_1[a], wR_2[b] [I>=2σ (*I*)]	0.0403, 0.1072
R_1, wR_2 [all data]	0.0495, 0.1112
$\Delta\rho$[c] /e·Å^{-3}	1.89, -1.63

[a] $R_1 = \Sigma||F_o| - |F_c||/\Sigma|F_o|$.

[b] $wR_2 = [\Sigma w(F_o^2 - F_c^2)^2/\Sigma w(F_o^2)^2]^{1/2}$.

[c] Maximum and minimum residual electron density.

Table S2 Bond angles and bond lengths of $(MHEA)_4Pb_3Br_{10}$.

Bond angles	Angle / °	Bond lengths	Length / Å
Br(2)−Pb(1)−Br(3)	84.12 (3)	Pb(1)−Br(2)	2.9331 (10)
Br(2)−Pb(1)−Br(5)	91.25 (3)	Pb(1)−Br(3)	3.0920 (11)
Br(2)−Pb(1)−Br(5)^{i}	177.21 (3)	Pb(1)−Br(4)	2.8419 (11)
Br(3)−Pb(1)−Br(5)^{i}	93.17 (3)	Pb(1)−Br(5)	2.9737 (10)
Br(4)−Pb(1)−Br(2)	93.18 (3)	Pb(1)−Br(5)^{i}	3.1265 (10)
Br(4)−Pb(1)−Br(3)	93.14 (3)	Pb(2)−Br(1)	3.0307 (11)
Br(4)−Pb(1)−Br(5)	92.82 (3)	Pb(2)−Br(2)^{ii}	3.0595 (12)
Br(4)−Pb(1)−Br(5)^{i}	87.63 (3)	Pb(2)−Br(3)	3.0044 (12)
Br(5)−Pb(1)−Br(3)	172.64 (3)		
Br(5)−Pb(1)−Br(5)^{i}	91.375 (10)		
Br(1)−Pb(2)−Br(1)^{ii}	170.94 (6)		
Br(1)−Pb(2)−Br(2)^{ii}	102.35 (3)		
Br(1)−Pb(2)−Br(2)	84.07 (3)		
Br(2)−Pb(2)−Br(2)^{ii}	91.28 (4)		
Br(3)−Pb(2)−Br(1)	83.87 (3)		
Br(3)−Pb(2)−Br(1)^{ii}	90.46 (3)		
Br(3)−Pb(2)−Br(2)	83.50 (3)		
Br(3)^{ii}−Pb(2)−Br(2)	171.48 (3)		
Br(3)−Pb(2)−Br(3)^{ii}	102.45 (5)		
Pb(1)−Br(2)−Pb(2)	83.43 (3)		
Pb(2)−Br(3)−Pb(1)	81.71 (3)		
Pb(1)−Br(5)−Pb(1)^{iii}	168.39 (4)		

Symmetry codes: (i) $-x-1/2, y-1/2, -z+1/2$; (ii) $-x, y, -z+1/2$; (iii) $-x-1/2, y+1/2, -z+1/2$.

Table S3. Summary of hydrogen bonds.

Hydrogen bonds for $(MHEA)_4Pb_3Br_{10}$				
D−H···A	D−H / Å	H···A / Å	D···A / Å	∠DHA / °
O(1)−H(1)···N(1)	0.82	2.58	2.933(15)	107
N(1)−H(1A)···Br(5)	0.89	2.55	3.378(8)	156
N(1)−H(1A)···O(1)	0.89	2.58	2.933(15)	104'

N(1)−H(1B)···Br(4)^{i}	0.89	2.61	3.365(9)	143
O(2)−H(2)···Br(3)^{ii}	0.82	2.70	3.468(11)	157
N(2)−H(2C)···O(1)	0.89	2.15	2.942(16)	148
N(2)−H(2C)···O(2)^{iii}	0.89	2.39	2.863(14)	114'
N(2)−H(2D)···O(2)	0.89	2.38	2.779(16)	107
N(2)−H(2D)···O(2)^{iii}	0.89	2.50	2.863(14)	105'
Symmetry codes: (i) *x*,2-*y*,1/2+*z*; (ii) -*x*,1+*y*,1/2-*z*; (iii) -*x*,3-*y*,1-*z*				

Table S4 Summary of the thermal properties of some reported 2D HMHs.

Compound	T_m	T_d	ΔT	Ref.
$(DMIPA)_2PbI_4$	98	243	145	[1]
$(MIPA)_2PbI_4$	117	245	128	[1]
$(1\text{-}MeHa)_2SnI_4$	142	228	86	[2]
$(MIBA)_2PbI_4$	136	219	82	[1]
$(GABA)_2PbI_4$	126	200	74	[3]
$(MIPTA)_2PbI_4$	138	213	73	[1]
$(R\text{-}NEA)_2PbBr_4$	168	204	36	[4]
$(1\text{-}Me\text{-}ha)_2PbI_4$	172	190	18	[5]
$(R/S\text{-}Cl\text{-}PEA)_2PbI_4$	222	239	17	[6]
$(2\text{-}Et\text{-}ha)_2PbI_4$	178	190	12	[5]
$(2\text{-}F\text{-}PEA)_2SnI_4$	201	208	7	[7]
$(Rac\text{-}Cl\text{-}PEA)_2PbI_4$	250	254	4	[6]
$(MHEA)_4Pb_3Br_{10}$	99	277	178	This work
$(DMBPA)_4Pb_3Br_{10}$	139	239	100	[8]
$(DMIPA)_4Pb_3I_{10}$	151	245	94	[8]
$(DMIEA)_4Pb_3I_{10}$	173	235	62	[8]

Reference

(1) Wang, W.; Liu, C. D.; Fan, C. C.; Fu, X. B.; Jing, C. Q.; Jin, M. L.; You, Y. M.; Zhang, W. Rational Design of 2D Metal Halide Perovskites with Low Congruent Melting Temperature and Large Melt-Processable Window. *J. Am. Chem. Soc.* **2024**, *146*, 9272-9284.

(2) Singh, A.; Crace, E.; Xie, Y.; Mitzi, D. B. A two-dimensional lead-free hybrid perovskite semiconductor with reduced melting temperature. *Chem. Commun.* **2023**, *59*, 8302-8305.

(3) Salah, M. B. H.; Mercier, N.; Dabos-Seignon, S.; Botta, C. Solvent-Free Preparation and Moderate Congruent Melting Temperature of Layered Lead Iodide Perovskites for Thin-Film Formation. *Angew. Chem. Int. Ed.* **2022**, *61*, e202206665.

(4) Singh, A.; Jana, M. K.; Mitzi, D. B. Reversible Crystal-Glass Transition in a Metal Halide Perovskite. *Adv. Mater.* **2021**, *33*, e2005868.

(5) Li, T.; Dunlap-Shohl, W. A.; Reinheimer, E. W.; Le Magueres, P.; Mitzi, D. B. Melting temperature suppression of layered hybrid lead halide perovskites via organic ammonium cation branching. *Chem. Sci.* **2019**, *10*, 1168-1175.

(6) Yang, C. K.; Chen, W. N.; Ding, Y. T.; Wang, J.; Rao, Y.; Liao, W. Q.; Tang, Y. Y.; Li, P. F.; Wang, Z. X.; Xiong, R. G. The First 2D Homochiral Lead Iodide Perovskite Ferroelectrics: [R- and S-1-(4-Chlorophenyl)ethylammonium]$_2$PbI$_4$. *Adv. Mater.* **2019**, *31*, e1808088.

(7) Mitzi, D. B.; Medeiros, D. R.; DeHaven, P. W. Low-Temperature Melt Processing of Organic−Inorganic Hybrid Films. *Chem. Mater.* **2002**, *14*, 2839-2841.

(8) Wang, W.; Liu, C. D.; Fan, C. C.; Zhang, W. Reversible Glass-Crystal Transition in a New Type of 2D Metal Halide Perovskites. *Adv. Funct. Mater.* **2024**, 2407143.